

SLAC - PUB - 3470  
October 1984  
(A)

Secondary Electron Yield and AES Measurements  
on Oxides, Carbide and Nitride of Niobium\*

E.L. GARWIN, E.W. HOYT, R.E. KIRBY

*Stanford Linear Accelerator Center  
Stanford University, Stanford, California, 94305*

and

T. MOMOSE

*KEK, National Laboratory for High Energy Physics  
Oho-Machi, Tsukuba-gun, Ibaraki-ken, 300-32, Japan*

ABSTRACT

Secondary electron yield measurements before and after Ar ion sputter cleaning were made on Nb and Nb compounds of interest for rf superconducting cavities. Total secondary electron yields ( $\sigma$ ) for primary energies 20-1500 eV were measured for solid Nb ( $\sigma$  max = 1.3 at 300 eV), anodized Nb<sub>2</sub>O<sub>5</sub> ( $\sigma$  max = 1.2 at 300 eV) and powders of: Nb ( $\sigma$  max = 1.0 at 400 eV), NbO ( $\sigma$  max = 0.9 at 400 eV), NbO<sub>2</sub> ( $\sigma$  max = 1.0 at 400eV), Nb<sub>2</sub>O<sub>5</sub> ( $\sigma$  max = 0.95 at 400 eV), NbC ( $\sigma$  max = 0.8 at 400 eV) and NbN ( $\sigma$  max = 0.8 at 500 eV). Determinations were made for Auger elemental sensitivities, and the relationship between Auger peak heights and oxide stoichiometry is discussed. The sputter etch rate of anodized Nb<sub>2</sub>O<sub>5</sub> was measured by depth profiling anodic coatings of known thickness.

Submitted to *Journal of Applied Physics*

---

\* Work supported by the Department of Energy, contract DE - AC03 - 76SF00515.

## 1. Introduction

The field of rf superconductivity has, for the last two decades, been presented with individual, tantalizing results which only now perhaps are developing into a mature technology. The maximum rf field attainable has been limited by thermal breakdown<sup>(1)</sup>, electron multipactoring<sup>(2)</sup>, or field emission<sup>(3)</sup>. Electron multipactor in simple cavities can be prevented by proper choice of the cavity shape<sup>(4)</sup>. Thermal breakdown is being pushed to higher gradient levels with the advent of purer materials from suppliers, and by purification schemes employing yttrium at modest temperatures on manufactured cavity parts<sup>(5)</sup>. Various dirt effects can be eliminated by carefully keeping the structures dust free after cleaning. After all the above has been said and done, surface effects are a major barrier to the maximum electric field gradient attainable in complex multicell structures, where local perturbations at couplers and turners may re-establish the possibility of multipactor. In addition, degradation of cavity performance upon exposure to air<sup>(6)</sup> must be minimized. At SLAC we are engaged in a detailed application of surface physics techniques to the study of Nb and its possible surface coatings. The objective is to produce a surface which is stable upon atmospheric exposure (or is renewable in situ) and has a low enough secondary emission coefficient to preclude multipactor.

The first step in this effort is to characterize the bare Nb surface with respect to its secondary emission properties. The effects of oxidation will be important and therefore we examine the various oxides of Nb. We also examine some candidate materials that might be used as overcoatings of Nb to reduce the secondary yield. Since room temperature oxidation of Nb typically leads to Nb<sub>2</sub>O<sub>5</sub> we have also examined anodic Nb<sub>2</sub>O<sub>5</sub> films as a model surface for oxidized Nb.

Auger electron spectroscopy (AES) is used to characterize the elemental composition of the surfaces studied here because it is an experimentally simple technique and is routinely used to determine surface cleanliness. Since chemi-

cal information is also available in the AES spectra, we searched for a possible relationship between the structure of the Nb transitions and the distribution of oxide states present.

The measurements presented here were performed in a standard unbaked UHV surface analysis system using a typical AES probe current of  $10 \mu\text{A}$ . This beam current is sufficient to cause some surface modification of dielectrics<sup>(7)</sup>. To reduce the beam current influence on the yield measurements, the current was reduced to  $10\text{nA}$  and the yield measurement was done on a point adjacent to the probing Auger beam.

## 2. Experiment

The experimental chamber is of standard cylindrical design and is constructed of type 304 stainless steel with an internal volume of approximately 100 liters. Measurements were performed at  $5 \times 10^{-9}$  to  $5 \times 10^{-10}$  torr without bakeout using a combination of ion and titanium sublimation pumping. A quadrupole residual gas analyzer monitored the system background and sputter Ar gas purity. The Ar was purified to better than 99.9% by reaction with HIP<sup>®</sup>-alloy<sup>(8)</sup> before admission to the system via a leak valve.

Sputter profiles were obtained using a commercial ion gun and cylindrical mirror analyzer.<sup>(9)</sup> The carousel accommodated samples with surface normals collinear with the axis of the coaxial electron gun of the CMA. The angle relative to the surface normal for ion bombardment was  $71^\circ$ . A 1 KeV unscanned sputter ion beam was used with a current density of  $62\mu\text{A}\cdot\text{cm}^{-2}$  in an Ar pressure of  $6 \times 10^{-5}$  torr. The FWHM of the ion beam current was 0.5 cm. The 2 KeV electron beam used for Auger analysis produced  $10 \mu\text{A}$  within a 0.021 cm diameter (10-90% width measurement, using a knife edge) for a current density of  $29 \text{mA}\cdot\text{cm}^{-2}$ .

Analog Auger spectra were recorded in differential mode, typically at 2 volts peak-to-peak modulation, 0.1 sec time constant and sweep rate of 17 eV-

sec<sup>-1</sup>. Spectra taken for sputter profiles were done in the presence of Ar with the ion beam off.

Total secondary yield ( $\sigma$ ) measurements were made using the retarding potential method of Henrich.<sup>(10)</sup> The cathode potential of the CMA electron gun was fixed at -1500 volts. The final electron energy arriving at the sample was determined by a negative retarding potential applied to the sample via the sample carousel. Accuracy in the electron beam energy was  $\pm 3$  eV. The incident beam current for yield measurements was set to 10 nA using a polycrystalline graphite target biased to +500 volts relative to the chamber, after the gun structure was thermally stabilized by cathode heating. Tests showed that the current remained stable to within 5% over the yield measurement time. By making several successive yield curve measurements on the sample, it was shown that essentially identical curves were obtained. This stability also reflects the minimal surface modification that is caused by this current density. We did, however, observe changes in successive yield curve measurements if beams of 5  $\mu$ A were used. The 10 nA ( $29\mu\text{A}\cdot\text{cm}^{-2}$ ) beam showed no such changes. Electron beam damage in native oxides<sup>(11)</sup> has been observed at 5 keV and  $2 \times 10^{-3}$  C $\cdot\text{cm}^{-2}$ , however, we have not observed such damage here at a dose ten times higher but at much lower average energy using the 10nA beam.

Yield curves were measured point by point, at 100 eV intervals above 100 eV and 10 eV intervals below 100 eV with total measurement time of 10 min/curve, and a total electron dose per curve of  $1 \times 10^{17}$  electron $\cdot\text{cm}^{-2}$ . Since a  $10\mu\text{A}$  beam was used for the Auger measurements, the beam was moved several beam diameters away from the point of Auger measurement to do the yield measurement and subsequently returned to the original spot for further Auger analysis.

### 3. Sample and Surface Preparation

The solid Nb samples were prepared from low-Ta (<350 ppm) electron-beam-melted Nb supplied by Teledyne Wah Chang Corporation. Sections were cut and machined from previously outgassed (2500 K) rods. These samples had extremely large grains ( $\approx 1$  cm), therefore, the resulting surfaces (1.25 cm diameter) were essentially single crystals 0.1 cm thick.

The Nb surfaces were degreased in Freon, polished mechanically with 0.5  $\mu$  diamond paste and then chemically etched in a 10% HF - 90% H<sub>2</sub>SO<sub>4</sub> solution to remove  $\approx 50\mu$  of surface.

To study Nb<sub>2</sub>O<sub>5</sub> layers, samples prepared as above were anodized to various thicknesses in 3% NH<sub>4</sub>OH solution using a pure Nb cathode. A value of 24 A/V<sup>(12,13)</sup> was used to calculate the oxide thickness. The anodizing voltage, held constant throughout the anodizing process,<sup>(12)</sup> was removed when the current fell to 1% of its initial value. The other solid samples used were thin foils of polycrystalline graphite and Ag. Powder samples of Nb, NbO, NbO<sub>2</sub>, Nb<sub>2</sub>O<sub>5</sub>, NbC and NbN were prepared for measurement by pressing the powders onto In-coated Cu disks. All of the powder samples were 1.3 cm diameter and 0.1 cm thick. Sample grain size and purity information is summarized in Table I. The reason for examining powders is that some of the compounds of interest were readily available as single-phase substances only in powder form.

Table I

Sample	Grain Size	Purity(%)	Supplier
Nb(Solid)	$\geq 1\text{cm}$	99.92	Wah Chang
Nb(Powder)	$> 300\mu$	99.8	Fansteel
Nb(Powder)	$< 75\mu$	99.8	Fansteel
NbO(Powder)	$< 150\mu$	99+	Thiokol
NbO <sub>2</sub> (Powder)	$< 75\mu$	99+	Thiokol
Nb <sub>2</sub> O <sub>5</sub> (Powder)	$< 45\mu$	99.99	Thiokol
Nb <sub>2</sub> O <sub>5</sub> (Anodic Layer)	Substrate $> 1\text{cm}$	99.92	Wah Chang
NbC(Powder)	$< 150\mu$	99+	Thiokol
NbN(Powder)	$< 150\mu$	99.9	Thiokol
Polycrystalline Graphite AXF-Q1	$\sim 5\mu$ thick foil	99.999	Poco
Silver(Solid)	$10\mu$ thick foil	99.99	Wesgo

## 4. Measurements

### 4.1 AUGER SENSITIVITIES

The Auger inverse sensitivity factors<sup>(14)</sup> for Nb(solid) and C(polycrystalline graphite) were determined by comparison to an elemental standard. The standard used in this procedure was a freshly sputter-cleaned Ag sheet, the Auger peak-to-peak height of which was measured during each experiment in order to determine the overall system gain. The sensitivity factors for sputter-cleaned Nb and C were determined as 0.78 and 0.34, respectively. These disagree with the values of 0.27 and 0.20 listed in Davis et al.<sup>(14)</sup> This discrepancy for Nb may arise because our Nb disks were large grained, essentially single crystal samples whose Auger emission might be expected to be strongly angular dependent. The cause of the difference in the C results could be due to the fact that we used graphite, rather than amorphous C.

The sensitivity factor for powdered Nb could not be determined because it was impossible to clean completely (Figure 3 and 4). The factors for the remaining materials were not calculated because sputtering alters the chemical composition of the surface making a determination impossible.<sup>(15)</sup> Results for the sputter etch profiles are thus given in peak-to-peak signal heights rather than atomic concentrations.

### 4.2 SPUTTER ETCH PROFILES

#### Anodic Nb<sub>2</sub>O<sub>5</sub>:

Auger spectra for sputter etch profiles were taken with Ar gas in the system and the ion beam off. Calibration of Ar ion sputter etch rates of Nb<sub>2</sub>O<sub>5</sub> was accomplished using anodically prepared coatings of various thicknesses over the range of 96 Å to 5400 Å. X-ray diffraction measurements on the thickest film confirmed that it was single phase Nb<sub>2</sub>O<sub>5</sub>. A typical sputter etch profile is shown in Figure 1 and the sputter etch calibration curve is shown in Figure 2. The ion bombardment time to the Nb<sub>2</sub>O<sub>5</sub>/Nb interface is determined as

the time necessary for the average oxygen concentration in the  $\text{Nb}_2\text{O}_5$  film to fall 50% at the  $\text{Nb}_2\text{O}_5/\text{Nb}$  interface. The calculated etch rate is approximately  $320 \text{ \AA}\cdot\text{mA}\cdot\text{cm}^{-2}\cdot\text{min}^{-1}$  for the conditions specified in Sec. 2

The profile of Figure 1 shows a small C buildup at the  $\text{Nb}_2\text{O}_5/\text{Nb}$  interface. The origin of this C is presumably due to air-borne contamination of the freshly etched Nb surface prior to anodization. Some of this C persists into the Nb bulk during sputtering. This effect is probably due to a combination of: 1) knock-on effects, 2) recontamination of the very active Nb surface with C-containing molecules from the gas phase and 3) the very low sputtering yield of C (which leads to surface segregation of the low-sputter-yield component).<sup>(15)</sup> The C concentration analyzed for our bulk Nb samples was  $<30$  ppm.

#### Powder Samples:

Depth profiles of the various powders studied in this work are shown in Figures 3-9. The O and C content is high, as expected, in the highly reactive Nb powder. The NbC and NbN samples are somewhat oxidized as well, even after sputtering. These effects suggest that the results for powders presented here may be indicative of, but certainly not identical to, data for solid material.

### 4.3 SECONDARY ELECTRON YIELDS

Total secondary electron yield data for the various solid and powder samples is presented in Figures 10-13. The "before sputtering" curves are for samples as-inserted into vacuum, while those "after sputtering" represent the point at which no further significant change in  $\sigma$  could be observed with further sputtering.

These equilibrium  $\sigma$  values were generally reached after short ion bombardment times of 1-10 minutes ( $3 \times 10^{16}$  to  $3 \times 10^{17}$  ions- $\text{cm}^{-2}$ ), and reflect the fact that the layer removed was probably the atmospheric contamination layer

present on the samples before insertion into vacuum. With continued sputtering, the yield values remained quite constant although the Auger spectra continued to change during removal of the remaining 10-20% of a monolayer or so of C and other contaminants in the case of anodized Nb<sub>2</sub>O<sub>5</sub>.

Figure 14 shows the results of  $\sigma$  measurements made on anodized Nb<sub>2</sub>O<sub>5</sub> at various stages of sputtering. The large change in  $\sigma$  upon removal of atmospheric contamination is quite evident, as well as its essentially unchanged value when the bulk of the Nb<sub>2</sub>O<sub>5</sub> is probed. As one sputters into the pure Nb layer, there is a substantial rise in the high energy portion of the curve which reflects an increase in the backscatter contribution to the yield. However, for energies below 300 eV, there is little difference between the yields of clean Nb and clean anodized Nb<sub>2</sub>O<sub>5</sub>.

Measurements on Nb and Nb<sub>2</sub>O<sub>5</sub> powders show  $\sigma$  values which are 20-30% lower than for the corresponding solid materials. This can be attributed to trapping of the secondary electrons in the powder matrix.<sup>(16)</sup> It is this morphologically produced effect which probably produces the flat yield in powders after removal of the atmospheric contamination layer.

#### 4.4 STOICHIOMETRY

Figure 15 shows a portion of typical Auger spectra for a sputter-cleaned anodic Nb<sub>2</sub>O<sub>5</sub> layer on Nb, both before and after sputtering through the anodic layer. There are some obvious changes in the peak structure which might be correlated with the chemical state of the Nb and then used to identify the presence of various Nb-oxide compounds on technical cavity surfaces.

Lin and Lichman<sup>(7)</sup> have shown that the "doublet" structure of Figure 15 is due to "oxide" and "metal" peaks in those transitions having final state Auger emissions in the Nb valence band. The doubling is obvious in the valence band transitions of Figure 15 while only small effects and no obvious doubling is observed in the lower lying (higher binding energy) transitions.

If the "metal" and "oxide" components of the valence doublets were sufficiently well separated in energy, an attempt could be made to correlate Nb peak heights with oxygen/Nb concentration or oxidation number<sup>(17)</sup>. Such a correlation is sometimes done in XPS where the core levels used are usually narrow and well resolved<sup>(18)</sup>. The situation for Auger spectra, at least in the Nb case, is very different. The line widths are 5-10 eV wide because of a combination of the broad final state valence band emission energy broadening due to short Auger transition times. Thus the distinct identity of the "oxide" and "metal" peaks is (due to overlap) not preserved for analysis. Electron and ion beam-induced decomposition of the surface oxides also act to further complicate the situation, separately from the line width consideration. The sputter profiles presented here use the total Nb transition at 170eV (including both "metal" and "oxide" components) because of the difficulty in separating the components.

While the presence of the doublets does provide a qualitative indication that Nb oxides do exist on the surface, monitoring the Auger oxygen peak is a simpler way of detecting oxygen on the surface.

## 5. Discussion

According to the literature, sputtering of Nb oxide surfaces apparently leads to a reduction in the oxide state,  $\text{Nb}_2\text{O}_5$  and  $\text{NbO}_2$  reduce to  $\text{NbO}$ <sup>(19-21)</sup> and  $\text{NbO}$  reduces to  $\text{NbO}_{0.7}$ <sup>(21)</sup>. The range of O/Nb of these sputtered surfaces of 0.7 to 1.0 is in conflict with our results, as discussed below.

Examination of the depth profiles of Figures 5, 6 and 7 shows that the sputtering time required to achieve equilibrium for the Nb oxide powders is in the order  $t_{\text{NbO}} > t_{\text{NbO}_2} > t_{\text{Nb}_2\text{O}_5}$ . This is not an oxide-state dependence but, rather is due to the grazing incidence angle of the sputtering beam to the powder surfaces which cleans up larger particle size (see Table I) slower because of shadowing effects.

Of more interest is the O/Nb ratio for these materials after having been sputtered to equilibrium: 0.9 for Nb<sub>2</sub>O<sub>5</sub>, 0.7 for NbO<sub>2</sub> and 0.4 for NbO. These are in the same ratio as the O/Nb stoichiometry, namely, 0.9 : 0.7 : 0.4 as 2.5 : 2 : 1 for Nb<sub>2</sub>O<sub>5</sub> : NbO<sub>2</sub> : NbO. This range of 2.5 : 1 for O/Nb is very different from that of 1 : 0.7 discussed above from the literature.

We believe that this disagreement is due to the depth of penetration of the incident ions<sup>(22)</sup>. An estimate<sup>(23)</sup> of the inelastic mean free path for O and Nb Auger electrons from inorganic compounds is 20 and 11 Å, respectively, for the analyzed energies used here. However, a calculation of the penetration depth of our ion beam using LSS theory<sup>(24-26)</sup>, with an average atomic mass for Nb<sub>2</sub>O<sub>5</sub> equal to 38, yields a value of 12 Å at normal incidence and 4 Å at the grazing incidence used here. So it is possible that the actual ion-damaged layer of NbO<sub>x</sub> is very thin and contributes significantly less to the Auger intensity in our spectra as compared to sputter-reduction studies previously published<sup>(19-21)</sup>, simply because the ion beam is at grazing incidence and low energy.

As a function of surface roughness, there is expected to be no dependence<sup>(27)</sup> of the O/Nb ratio for a given compound. merely as a function of surface roughness<sup>(27)</sup>. Absolute intensity however, should decrease as the roughness increases and, indeed, the individual O and Nb signals of the smooth anodized Nb<sub>2</sub>O<sub>5</sub> layer of Figure 1 are larger than those of the powdered Nb<sub>2</sub>O<sub>5</sub> sample of Figure 7.

## 6. Conclusion

The measurements reported here were followed by studies on sputter-deposited metalloids (TiN, TiC, NbN, NbC) conducted with more sophisticated equipment using very low probe currents, pulse counting techniques and dedicated computer manipulation of data<sup>(28)</sup>. The present measurements do indicate considerable promise of achieving Nb surfaces with low secondary electron emission. NbN and NbC look especially promising in this regard. We estimate that perhaps 20-25% of the secondary electrons are trapped by the powders, which implies that values close to unity should be achievable with solid NbC and NbN. TiN is routinely used at SLAC (because of its relatively low secondary electron yield) to coat various rf components for vacuum use.<sup>(29)</sup>

## 7. References

1. J.P. Turneaure and I. Weissman, J. Appl. Phys. 39, 4417 (1968).
2. P. Kneisel, O. Stoltz and J. Halbritter, J. Appl. Phys. 44, 1785 (1973).
3. I. Ben-Zvi, J.F. Crawford and J.P. Turneaure, IEEE Trans. Nucl. Sci. NS-20, 54(1973).
4. Ph. Bernard, G. Cavallari, E. Chiaveri, E. Haebel, H. Heinrichs, H. Lengeler, E. Picasso, V. Picciarelli and J. Tueckmantel, Nucl. Instrum. Meth. 190, 257 (1981); Ph. Bernard, G. Cavallari, E. Chiaveri, E. Haebel, H. Lengeler, H. Padamsee, V. Picciarelli, D. Proch, A. Schwettman, J. Tückmantel, W. Weingarten and H. Piel, Nucl. Instrum. Meth. 206, 47(1983).
5. H. Lengeler, W. Weingarten, G. Müller and H. Piel, IEEE Trans. on Magnetics 21, 1014 (1985); H. Padamsee, IEEE Trans. on Magnetics 21, 149 (1985).
6. T. Furuya, S. Hiramatsu, T. Nakazato, T. Kato, P. Kneisel, Y. Kojima and T. Takagi, IEEE Trans. Nucl. Sci. NS-28, 3225(1981).
7. T.T. Lin and D. Lichtman, J. Mat. Sci. 14, 455 (1979).
8. Hydrogenous impurity protection alloy. Vallecitos Nuclear Center, General Electric Co.
9. Varian Cylindrical Mirror Analyzer Model 981-2067, Varian Ion Bombardment Gun Model 981-2046.
10. V.E. Henrich, Rev. Sci. Instrum. 45, 861(1974).
11. C.G. Pantano and T.E. Madey, Appl. Surf. Sci., 7, 115(1981).
12. Y.L. Chiou, Thin Solid Films, 8, R37(1971).
13. T.W. Hickmott, J. Appl. Phys., 37, 4380 (1966).

14. L.C. Davis, N.C. MacDonald, P.W. Palmberg, G.E. Riach and R.E. Weber, *Handbook of Auger Electron Spectroscopy*, 2nd Ed., PHI Industries (1976).
15. G. Betz and G.K. Wehner, in: *Sputtering by Particle Bombardment II*, R. Behrisch, ed., Springer-Verlag, New York (1983).
16. S. Flügge, *Handbuch der Physik*, Vol. XXI, 261, Springer-Verlag, Heidelberg(1956).
17. C.R. Brundle, *Surface Sci.* 52, 426 (1975); F.J. Szalkowski and G.A. Somorjai, *J. Chem. Phys.* 56, 6097 (1972); F.J. Szalkowski and G.A. Somorjai, *Surface Sci.* 52, 431(1975).
18. M.K. Bahl, *J. Phys. Chem. Solids* 36, 485(1975).
19. D.K. Murti and Roger Kelly, *Thin Solid Films* 33, 149(1976).
20. M. Grundner and J. Halbritter, *J. Appl. Phys.* 51, 397(1980).
21. P.C. Karulkar, *J. Vac. Sci. Technol.* 18 169(1981).
22. P.H. Holloway and R.S. Bhattacharya, *Surf. Interface Anal.* 3, 118(1981).
23. M.P. Seah and W.A. Dench, *Surf. Interface Anal.* 1, 2(1979).
24. H.E. Schiott, *Rad. Eff.* 6, 107(1970).
25. P. Sigmund and J.B. Sanders, *Int. Conf. on Appl. of Ion Beams to Semiconductor Technology*, Grenoble, 1967.
26. M.A. Taubenblatt and C.R. Helms, *J. Appl. Phys.* 54, 2667(1983).
27. O.K.T. Wu and E.M. Butler, *J. Vac. Sci. Technol.* 20, 453(1982).
28. To be submitted for publication.
29. I.E. Campisi, H. Deruyter, Z.D. Farkas, E.L. Garwin, H.A. Hogg, F. King and R.E. Kirby, *IEEE Trans. Nucl. Sci.*, NS - 30, 3363(1983).

## 8. Figure Captions

1. Typical sputter profile of 960 Å anodic Nb<sub>2</sub>O<sub>5</sub>. The Nb peak monitored is the total M<sub>4,5</sub>N<sub>2,3</sub>V transition (both oxide and metal components at ~170eV).
2. Sputter calibration curve for anodic Nb<sub>2</sub>O<sub>5</sub>. Non-zero vertical axis intercept due to presence of surface contamination on as-inserted films, e.g. see Figure 1.
3. Sputter profile for <200 mesh Nb powder.
4. Sputter profile for >48 mesh Nb powder.
5. Sputter profile for NbO powder.
6. Sputter profile for NbO<sub>2</sub> powder.
7. Sputter profile for Nb<sub>2</sub>O<sub>5</sub> powder.
8. Sputter profile for NbC powder.
9. Sputter profile for NbN powder.
10. Secondary electron emission yield for >48 mesh Nb powder and solid Nb.
11. Secondary electron emission yield for NbO and NbO<sub>2</sub> powders.
12. Secondary electron emission yield for Nb<sub>2</sub>O<sub>5</sub> powder and anodic layer.
13. Secondary electron emission yield for NbC and NbN powders. Yield of polycrystalline graphite shown for comparison.
14. Secondary electron emission yield while sputtering through an 1100Å anodized Nb<sub>2</sub>O<sub>5</sub> layer into the underlying Nb bulk: ●-as inserted, ×-30 sec sputtering, ○-22 min sputtering, ▽-53.5 min sputtering (interface), □-250 min sputtering (Nb bulk).
- 15. Auger transitions for clean anodized Nb<sub>2</sub>O<sub>5</sub> and Nb.

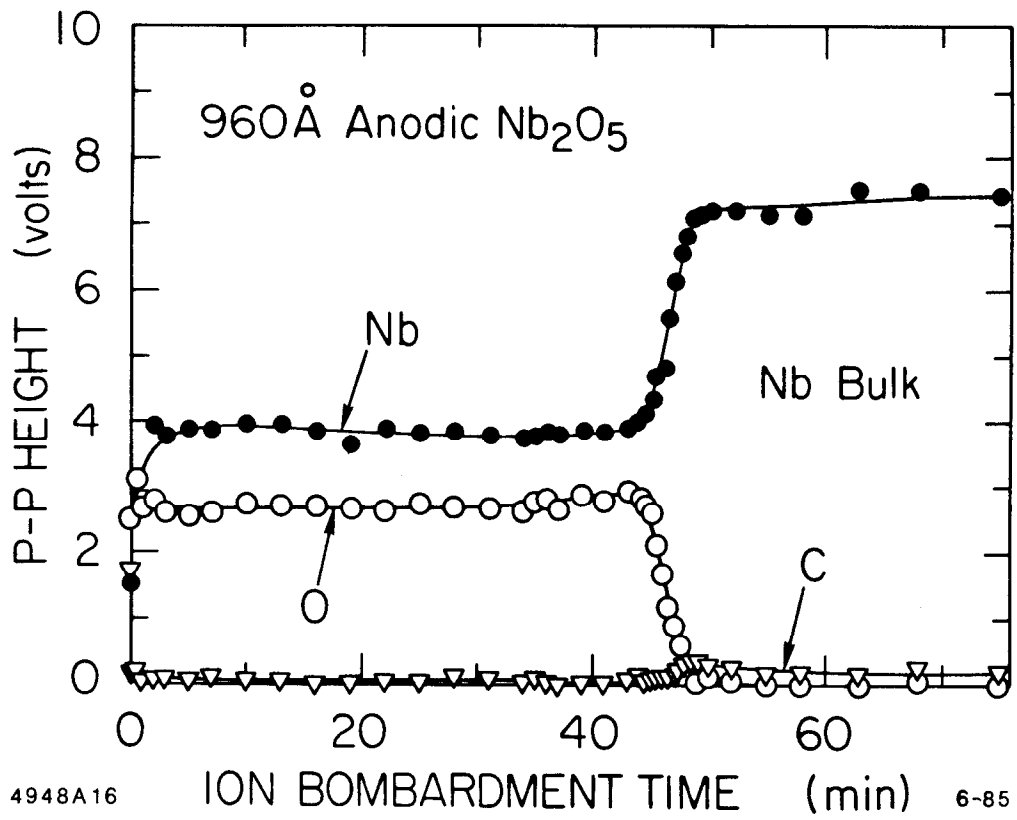


Fig. 1

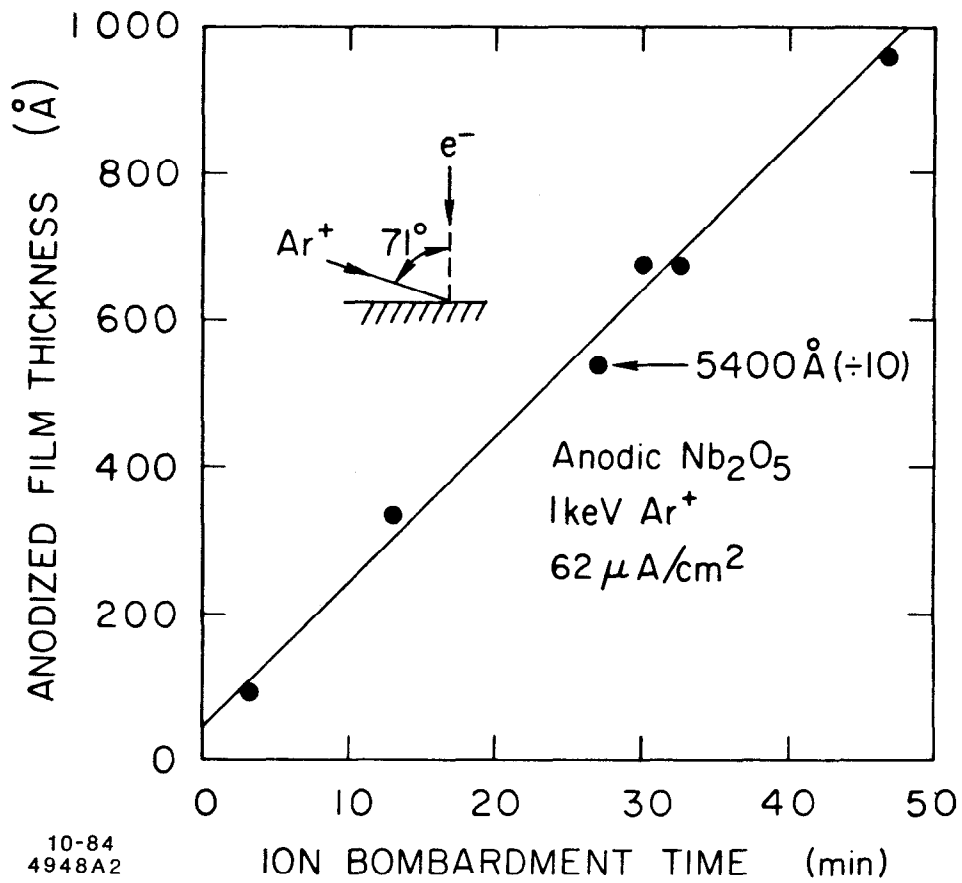


Fig. 2

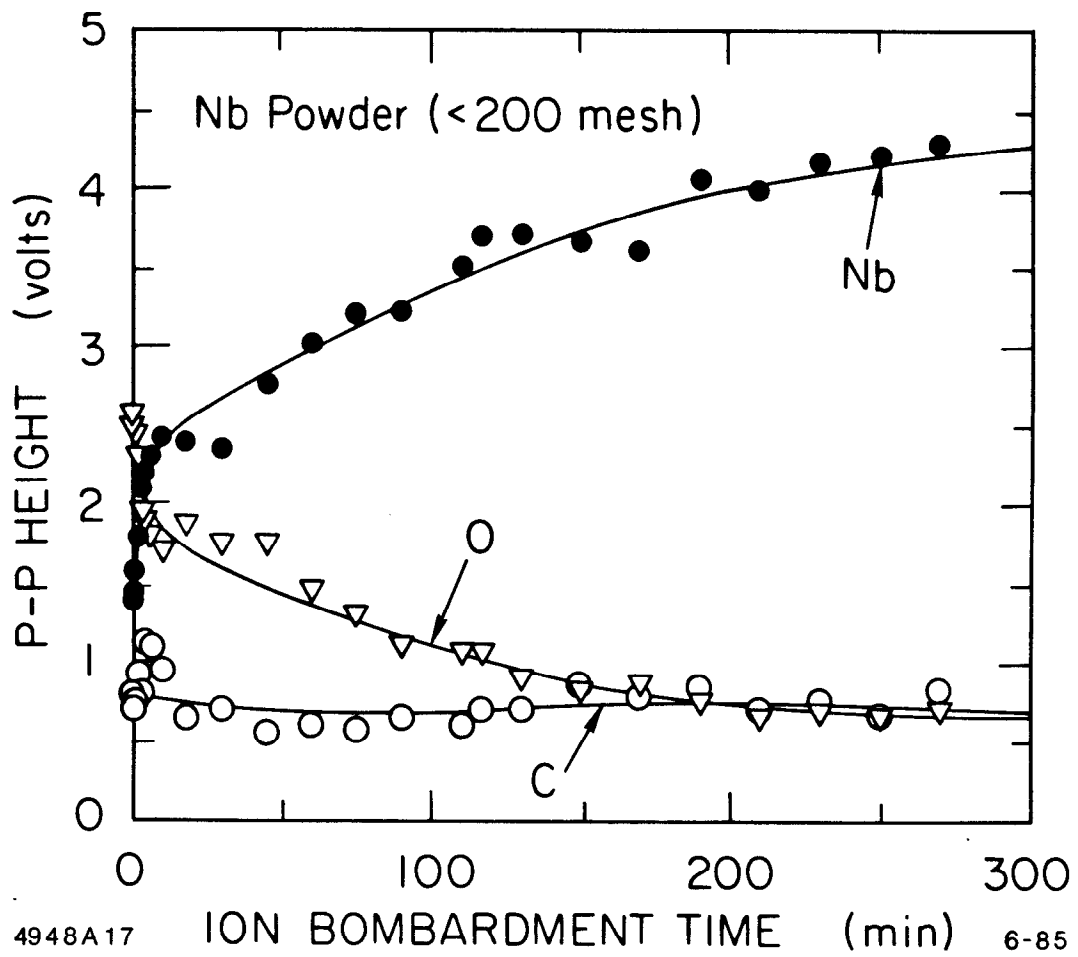


Fig. 3

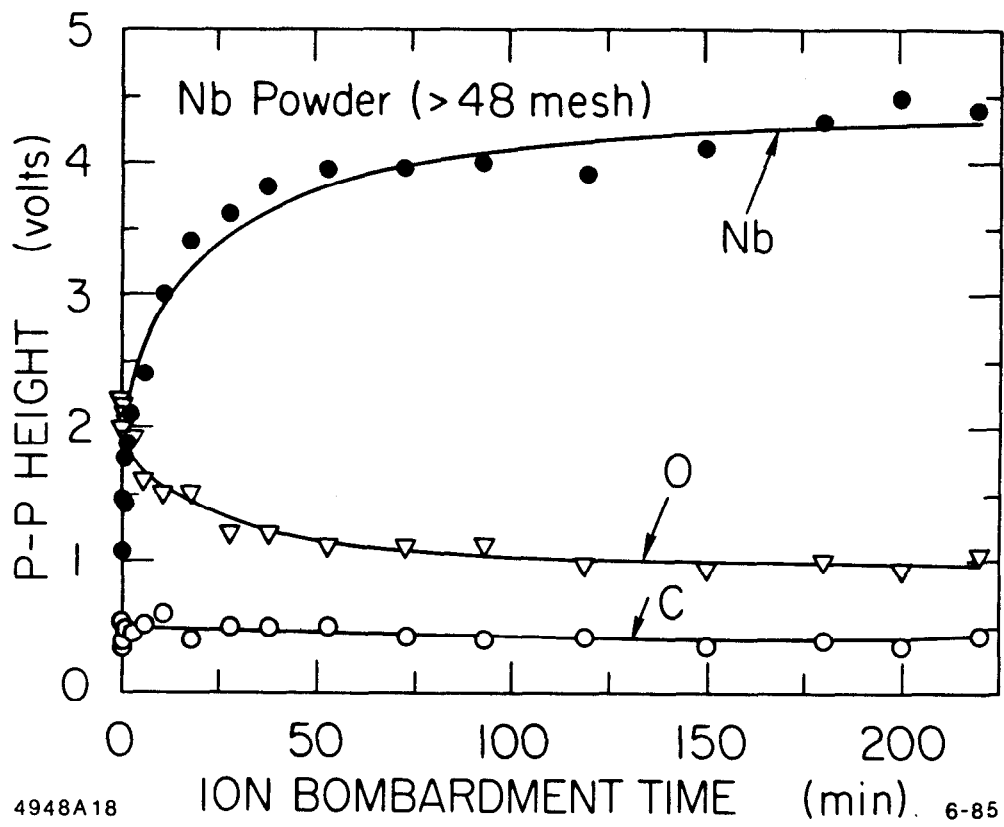


Fig. 4

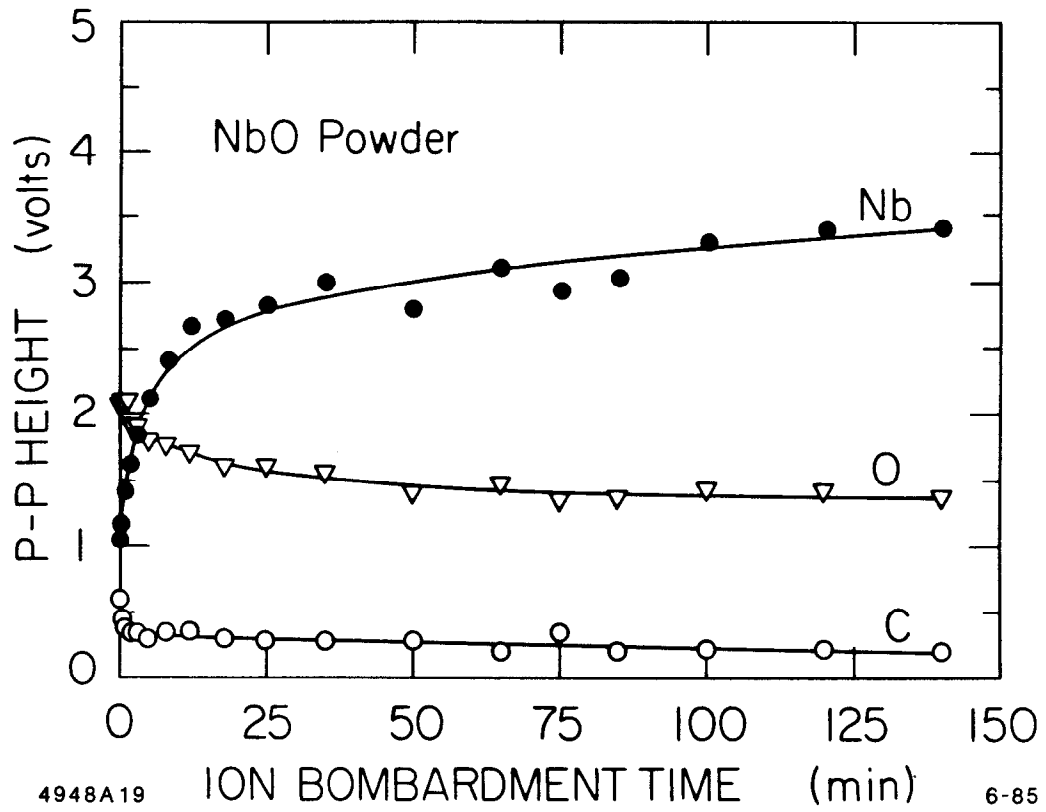
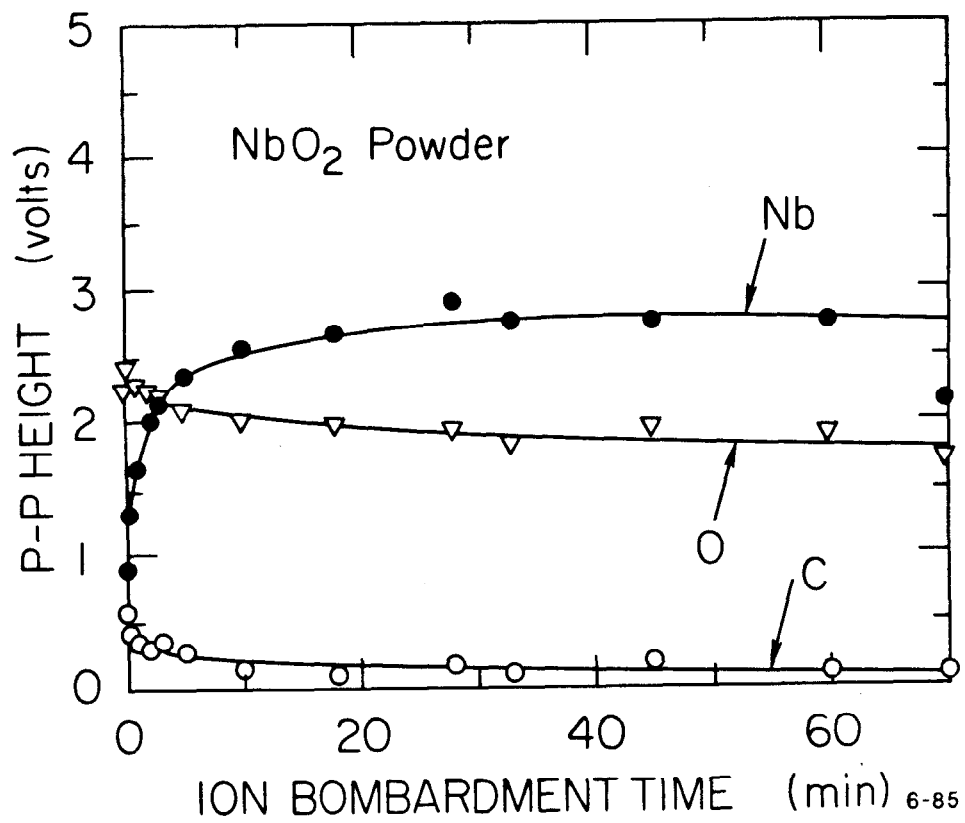


Fig. 5



4948A20

Fig. 6

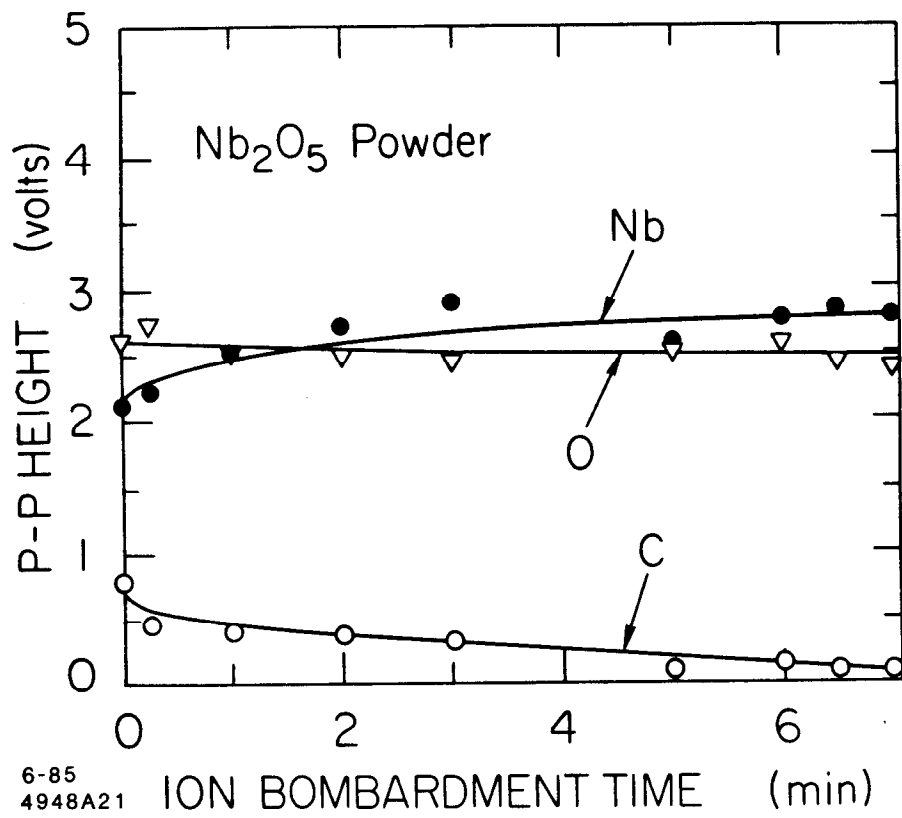


Fig. 7

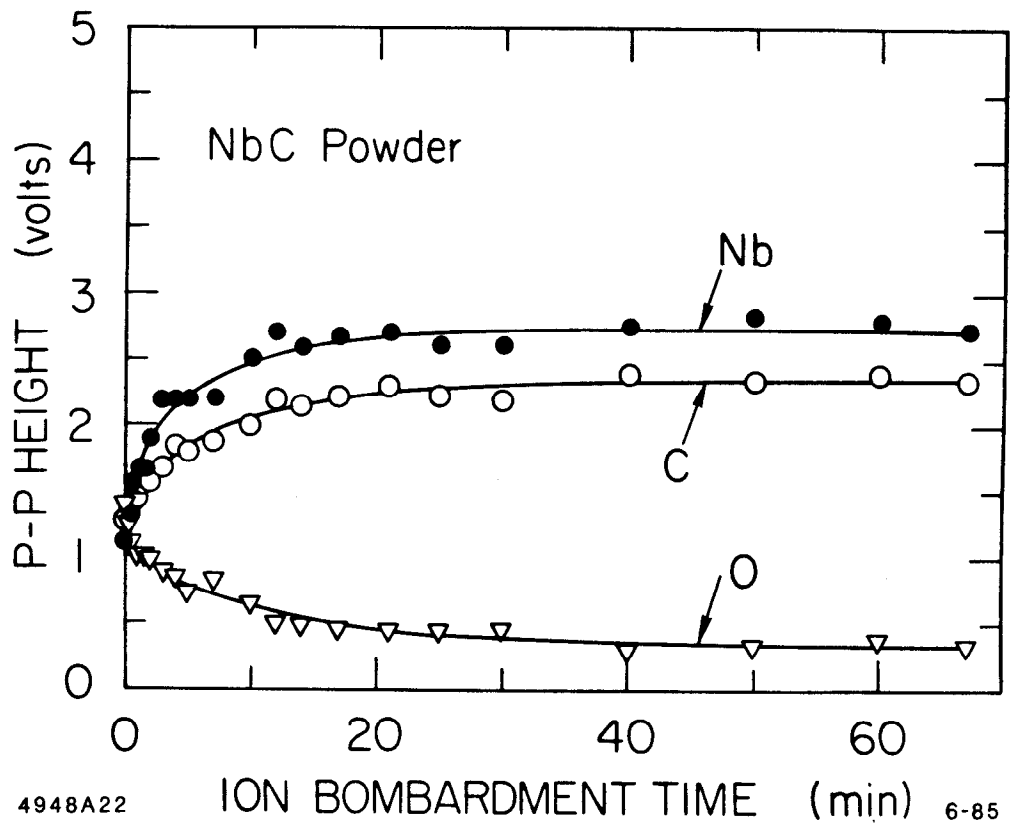


Fig. 8

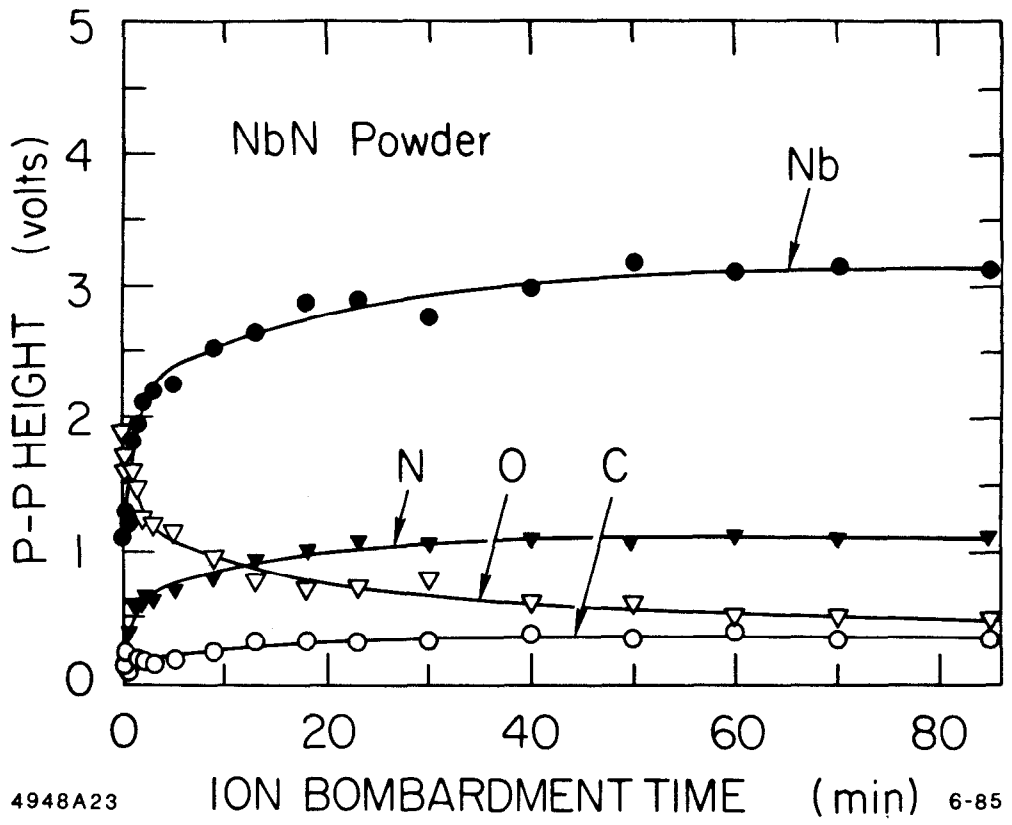
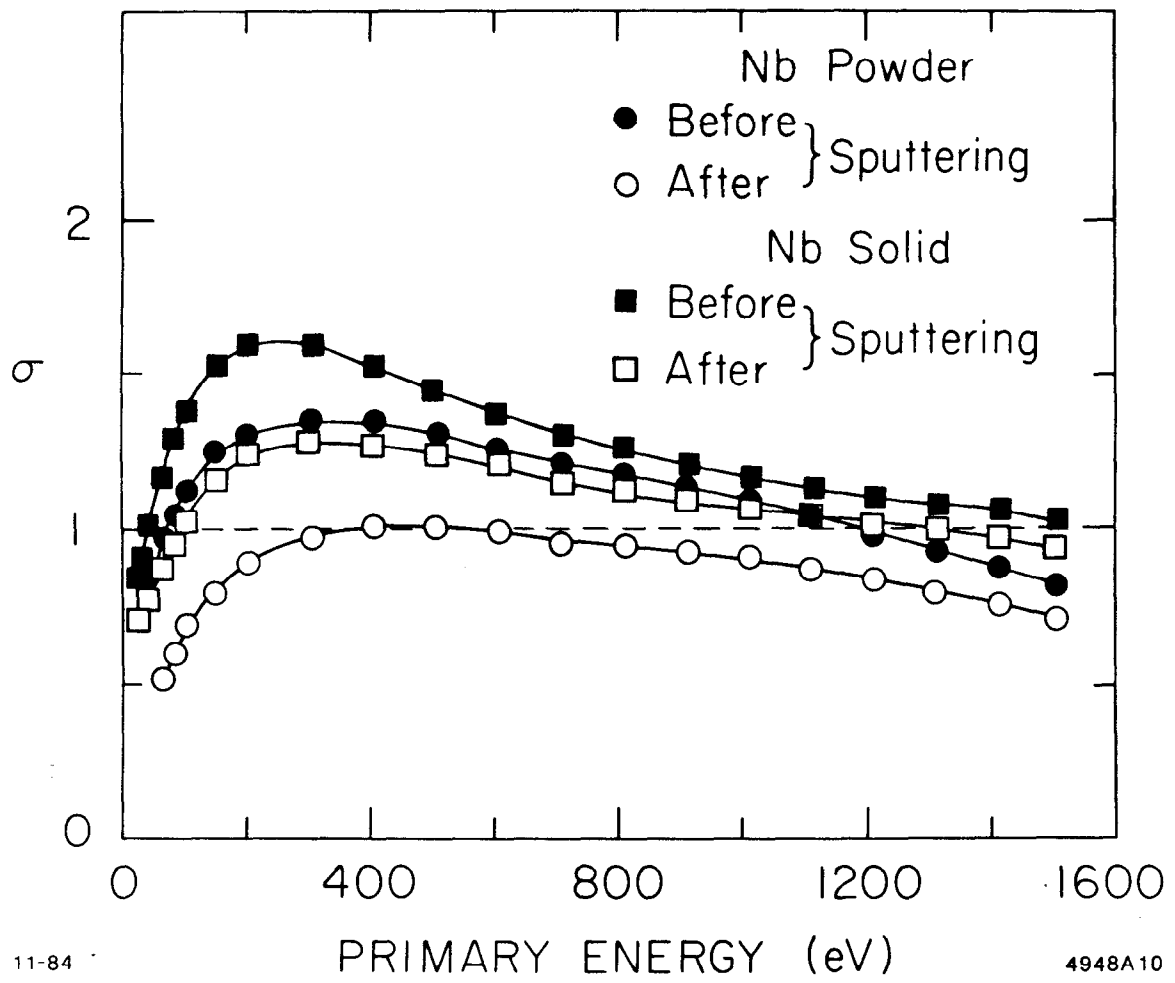


Fig. 9



11-84

4948A10

Fig. 10

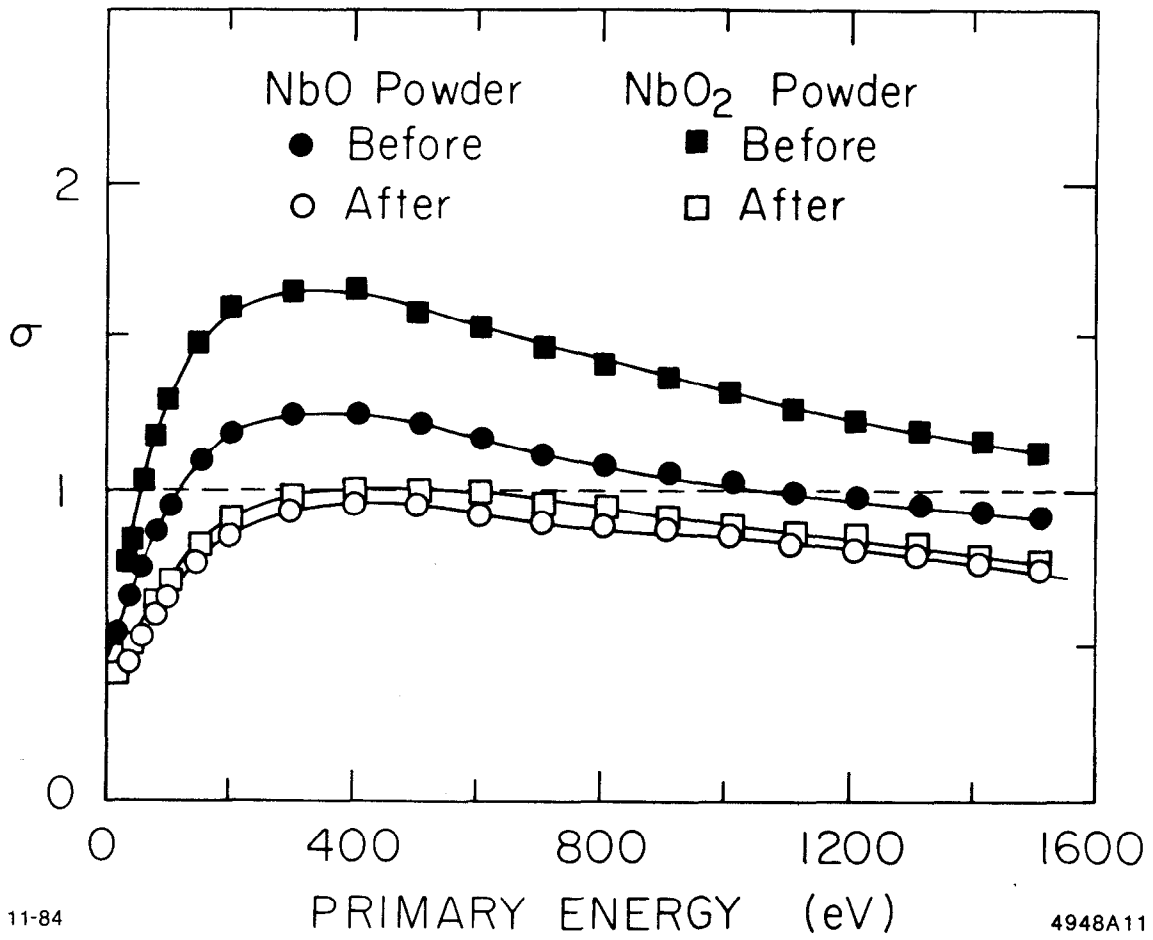


Fig. 11

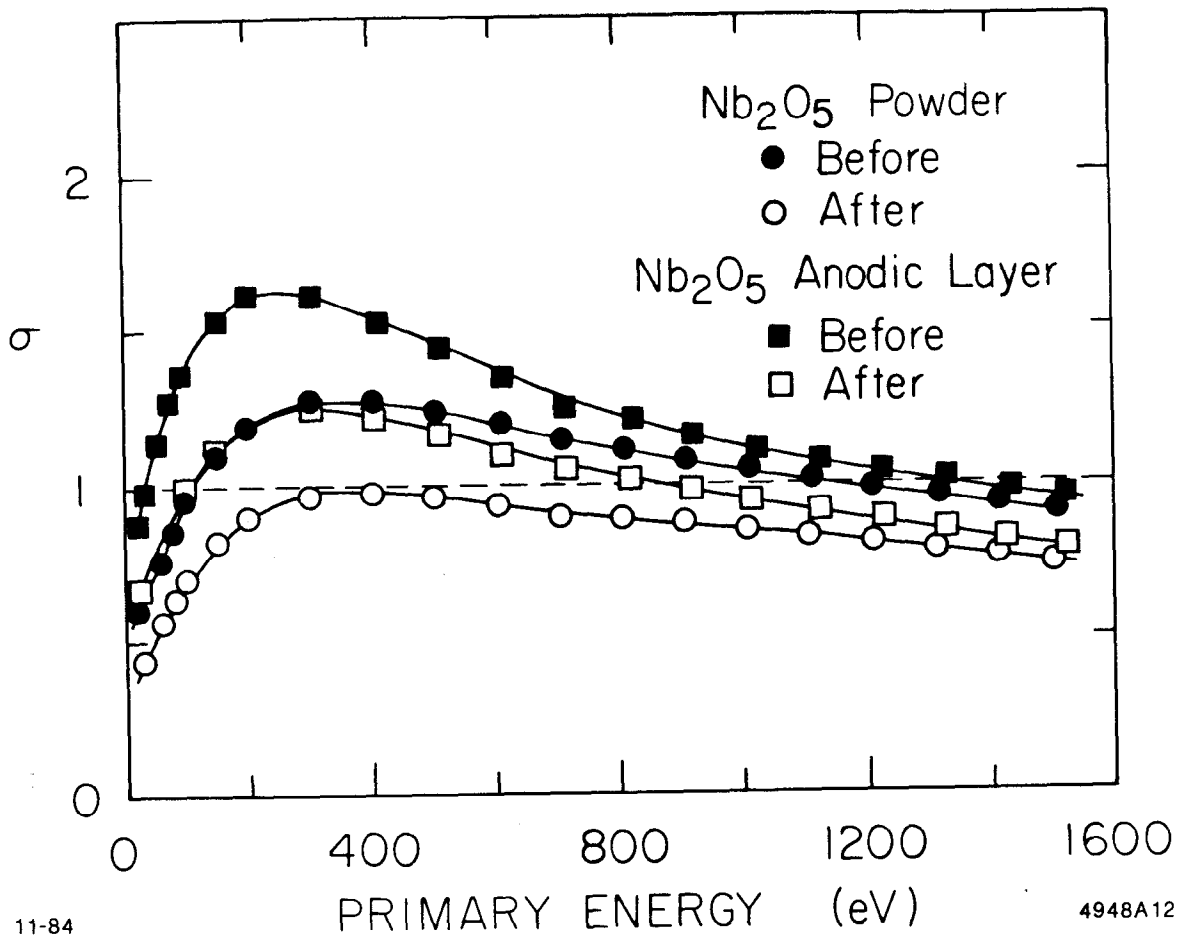


Fig. 12

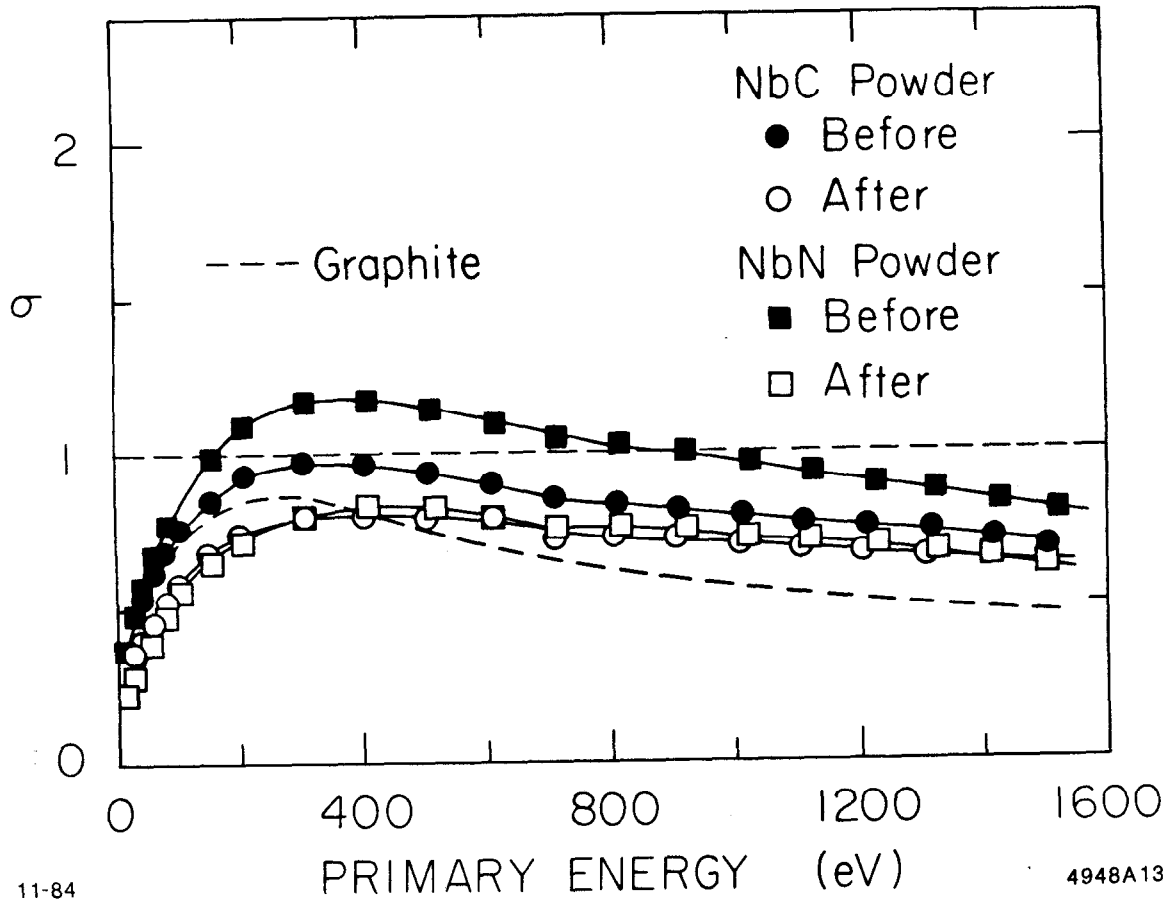


Fig. 13

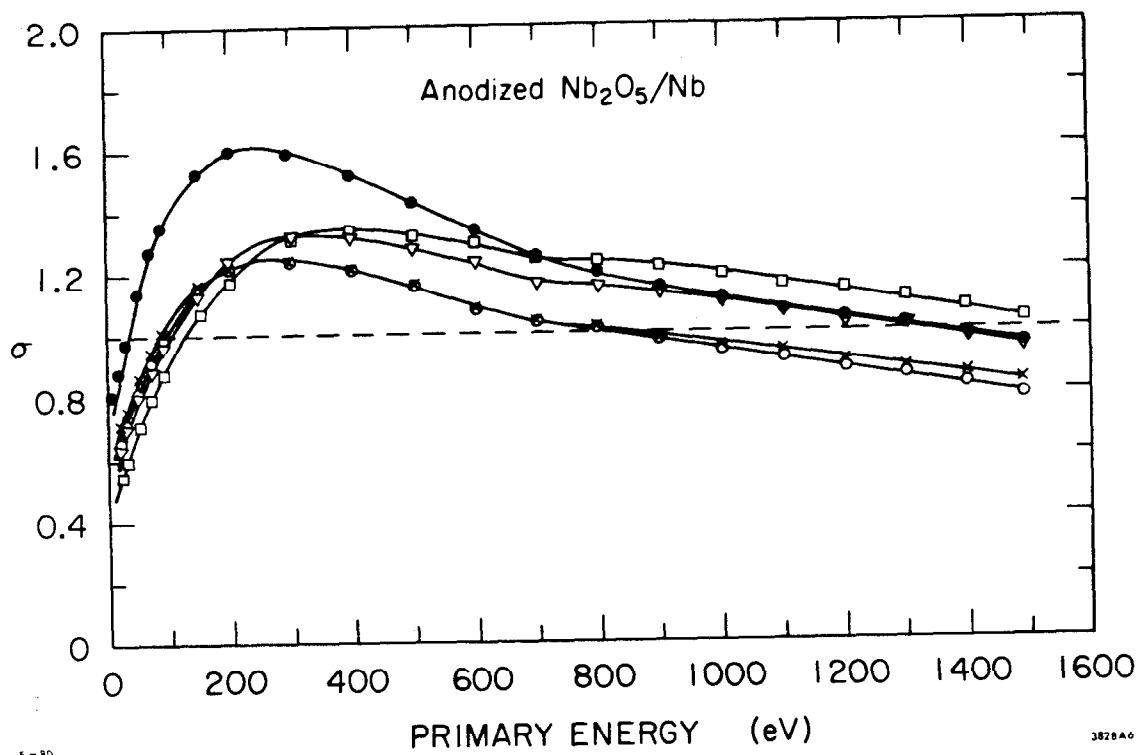


Fig. 14

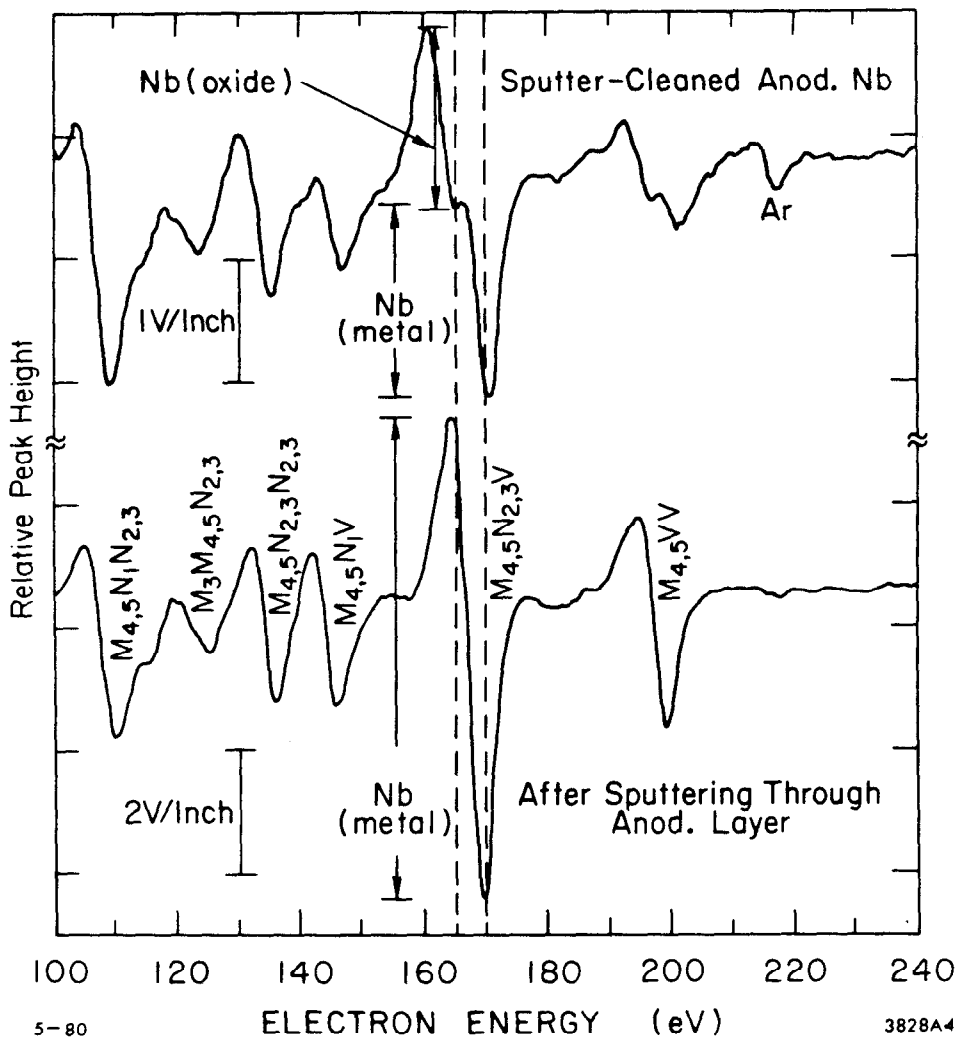


Fig. 15